Computational Mechanics 14 (1994) 68–83 © Springer-Verlag 1994

The application of interface elements and enriched or rate-dependent continua to micro-mechanical analyses of fracture in composites

J. C. J. Schellekens, R. de Borst

Abstract Micromechanical analyses are presented of matrix fracture and fibre-matrix debonding in carbon-epoxy composites. The fibres and the matrix are connected by special interface elements which allow for a geometric discontinuity (debonding) to arise. Two different models for the fibres and the matrix of the composite structure are used: firstly an elasto-plastic Cosserat continuum and secondly a visco-plastic continuum. In the micro-mechanical analyses of matrix fracture it is demonstrated that, upon mesh-refinement, the load deflection curves converge to a unique solution when these regularised continua are applied, and that the width of the localisation band remains finite. When the interaction between matrix cracking and debonding is investigated the same observations hold.

1 Introduction

The structural performance of fibre-reinforced materials depends to a major extent upon the interfacial bonding between fibres and matrix material. Debonding often marks the onset of matrix cracking and may play a crucial role in the locations at which matrix cracking is initiated. At further stages of the loading process we observe joining of matrix cracks as well as of matrix cracks and debonded fibre-matrix interfaces until complete loss of structural integrity finally occurs.

To obtain qualitative information on the progress of debonding and the influence of the interfacial bond properties on the structural performance of the composite material micromechanical analyses can be carried out. In numerical micromechanical analyses the fibres as well as the matrix are modelled by continuum elements and the interface is represented by special interface elements (Ngo and Scordelis 1967; Goodman et al. 1968; Schäfer 1975; Beer 1985; Rots 1988; Schellekens 1992; Schellekens and de Borst 1993a). In the undamaged state (fully bond) a sufficiently high dummy stiffness ensures that no additional deformations occur in the interface, which is assumed to have a zero thickness. After the tensile strength, or another equivalent strength measure, has been exceeded, the originally fully intact area gradually evolves into a geometric discontinuity, i.e. an internal stress-free boundary (at full debonding). In the formulation chosen here the strength/stiffness degradation occurs gradually. During the debonding process energy is dissipated. The quintessence of the approach for debonding is that the amount of dissipated energy is assumed to be equal to the critical energy release rate G_c of the interface that fractures. This model ensures a correct energy dissipation during debonding, so that below a certain discretisation, the crack propagation is independent of the fineness of the mesh. At the same time, the model results in a correct treatment of size effects (Schellekens 1992; Schellekens and de Borst 1993b).

The strength degradation in the matrix is modelled using a strain-softening Von Mises plasticity model. An inherent difficulty of any strain-softening model when utilised in a standard,

Communicated by B. Schrefler, 3 December 1993

J. C. J. Schellekens, R. de Borst
Delft University of Technology, Department of Civil Engineering,
P.O. Box 5048, 2600 GA Delft, The Netherlands

Correspondence to: J. C. J. Schellekens

The calculations presented in this paper have been carried out using the DIANA finite element package of TNO Building and Construction Research (TNO-BOUW)

rate-independent continuum setting is, that under quasi-static loading conditions the field equations cease to be elliptic. Well-posedness of the rate boundary value problem is lost and the mathematical model is no longer a proper description of the physics. In finite element simulations this loss of well-posedness becomes apparent through an extreme mesh sensitivity. Near failure all deformation concentrates in the smallest possible zone that can be resolved by the grid. Upon mesh refinement the failure zone collapses into a discrete plane (localisation) and the energy consumption during the failure process tends to zero. When the failure zone is known in advance interface elements as also used for the fibre-matrix interface can be located at the expected crack path. Together with a specification of the fracture energy that is dissipated in the crack a mesh-insensitive numerical solution can then be obtained.

If the crack path is not known in advance, two solutions are possible. Firstly, one can adaptively remesh during the non-linear process such that the correct crack path is aligned with the element boundaries (Larsson 1990). Secondly, and this approach is followed here, enriched or rate-dependent continuum models can be adopted (commonly named regularisation strategies). The two methods that will be adopted in this contribution to regularise the strain-softening Von Mises plasticity model are the Cosserat continuum (E. and F. Cosserat 1909; Günther 1958; Schäfer 1962; Mühlhaus and Vardoulakis 1987) and visco-plasticity (Loret and Prevost 1990; Sluys 1992). Both approaches intrinsically introduce an internal length scale in the continuum and have the effect that the rate boundary value problem remains well-posed also after the onset of strain softening for the matrix material. Accordingly, physically meaningful numerical solutions can be obtained.

The paper is organised as follows. Firstly, a concise treatment is given of the continuum models that have been used to model the matrix. The Cosserat approach and the visco-plastic model are briefly recapitulated. Then, the interface elements and the constitutive model for the debonding process are described in detail, whereby allowance is made for the rotational degrees of freedom that emerge in the Cosserat continuum description. Finally, a typical example is analysed in detail, whereby ample attention is given to issues like the sensitivity of the solution to mesh refinement and the interaction between debonding and matrix cracking.

2
Formulation of the elasto-plastic Cosserat continuum

In this section we will present the derivation of the element stiffness matrix for Cosserat elements in a plane deformation state. Furthermore a softening plasticity model based on a J_2 flow theory is included. A detailed description of the radial return algorithm employed to integrate the plastic strain rate vector and the associated consistent tangent stiffness relation for the elasto-plastic Cosserat continuum has been given in De Borst (1991). For more elaborate discussions on the Cosserat continuum the reader is referred to Günther (1958), Schäfer (1962), Mühlhaus and Vardoulakis (1987), Mühlhaus (1988–1990).

2.1
Element formulation

As already mentioned in the introduction the salient feature of a Cosserat continuum is that the set of translational degrees of freedom is augmented by nodal rotations, which introduces a length scale parameter in the continuum formulation. In a two-dimensional continuum the kinematic relations are defined as

$$\varepsilon_{11}=\frac{\partial u_1}{\partial x_1} \quad \varepsilon_{12}=\frac{\partial u_2}{\partial x_1}-\omega_3 \quad \kappa_{13}=\frac{\partial \omega_3}{\partial x_1} \quad \varepsilon_{22}=\frac{\partial u_2}{\partial x_2} \quad \varepsilon_{21}=\frac{\partial u_1}{\partial x_2}+\omega_3 \quad \kappa_{23}=\frac{\partial \omega_3}{\partial x_2} \tag{1}$$

with ω_3 the micro-rotation around the x_3-axis (see Fig. 1), $u_{(i)}$ the continuous displacements and κ_{13} and κ_{23} the micro-curvatures. In a similar fashion we can define the conjugate stress components σ_{11}, σ_{22}, σ_{33}, σ_{12}, σ_{21}, and moment-stresses m_{13} and m_{23} (see Fig. 1) which are conjugate to the micro-curvatures. Note that due to the introduction of the micro-rotations the stress and strain tensor are in general non-symmetric. If the nodal displacement vector $\boldsymbol{a}$ is defined as

$$\boldsymbol{a}=(a_1^1, a_1^2, \ldots, a_1^{nno}, a_2^1, a_2^2, \ldots, a_2^{nno}, \omega_3^1, \omega_3^2, \ldots, \omega_3^{nno})^T, \tag{2}$$

the strain tensor $\boldsymbol{\varepsilon}=(\varepsilon_{11}, \varepsilon_{22}, \varepsilon_{33}, \varepsilon_{12}, \varepsilon_{21}, \kappa_{13}, \kappa_{23})^T$ can be determined according to

$$\boldsymbol{\varepsilon}=\boldsymbol{B}\boldsymbol{a} \tag{3}$$

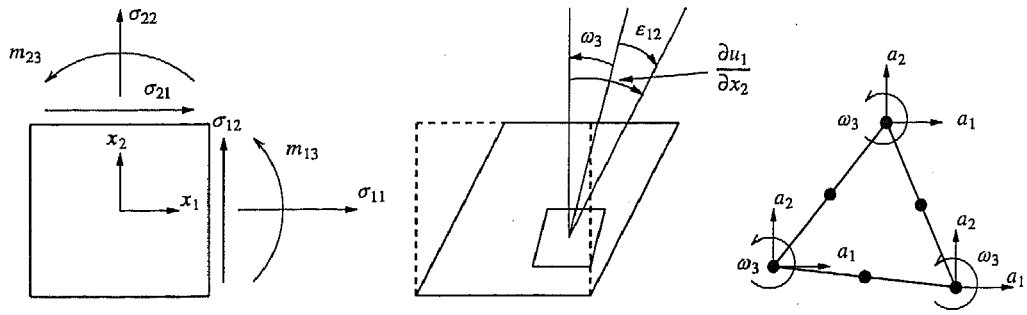

Fig. 1. Statics and kinematics for a Cosserat continuum

where the strain-displacement matrix B reads:

$$B^T = \begin{bmatrix} \frac{\partial n}{\partial x_1} & 0 & 0 & 0 & \frac{\partial n}{\partial x_2} & 0 & 0 \\ 0 & \frac{\partial n}{\partial x_2} & 0 & \frac{\partial n}{\partial x_1} & 0 & 0 & 0 \\ 0 & 0 & 0 & -n & +n & \frac{\partial n}{\partial x_1} & \frac{\partial n}{\partial x_2} \end{bmatrix}. \tag{4}$$

where $n = (N_1, N_2, \ldots, N_{nno})^T$ are the interpolation functions.

For plane deformations the matrix D_C that relates the elastic strain tensor to the stress tensor $\sigma = (\sigma_{11}, \sigma_{22}, \sigma_{33}, \sigma_{12}, \sigma_{21}, m_{13}, m_{23})^T$, is given by

$$D_C = \begin{bmatrix} 2\mu c_1 & 2\mu c_2 & 2\mu c_2 & 0 & 0 & 0 & 0 \\ 2\mu c_2 & 2\mu c_1 & 2\mu c_2 & 0 & 0 & 0 & 0 \\ 2\mu c_2 & 2\mu c_2 & 2\mu c_1 & 0 & 0 & 0 & 0 \\ 0 & 0 & 0 & \mu+\mu_c & \mu-\mu_c & 0 & 0 \\ 0 & 0 & 0 & \mu-\mu_c & \mu+\mu_c & 0 & 0 \\ 0 & 0 & 0 & 0 & 0 & 2\mu l_c^2 & 0 \\ 0 & 0 & 0 & 0 & 0 & 0 & 2\mu l_c^2 \end{bmatrix} \tag{5}$$

with $c_1 = (1-\nu)/(1-2\nu)$ and $c_2 = \nu/(1-2\nu)$ respectively. We observe that two parameters, additional to the conventional elasticity constants μ (shear modulus) and ν (Poisson's ratio), enter the continuum formulation: μ_c, the Cosserat shear modulus and l_c, a length parameter which is the essential feature of the Cosserat continuum model. The term $2\mu l_c^2$ can be considered as the bending modulus (Schäfer 1962). Finally, with B and D_C the element stiffness matrix can be determined as:

$$K = \int_S B^T D_C B \, dS. \tag{6}$$

with S the element surface.

2.2
Cosserat elasto-plasticity

For a J_2-flow theory the yield condition Φ^{pl} can be written as

$$\Phi^{pl} = ((3/2)\, \sigma^T P \sigma)^{1/2} - \bar{\sigma}(\kappa), \tag{7}$$

with $\bar{\sigma}$ the equivalent yield stress which is a function of a hardening/softening parameter κ and P the

projection matrix given by (De Borst 1991):

$$P = \begin{bmatrix} 2/3 & -1/3 & -1/3 & 0 & 0 & 0 & 0 \\ -1/3 & 2/3 & -1/3 & 0 & 0 & 0 & 0 \\ -1/3 & -1/3 & 2/3 & 0 & 0 & 0 & 0 \\ 0 & 0 & 0 & 1/2 & 1/2 & 0 & 0 \\ 0 & 0 & 0 & 1/2 & 1/2 & 0 & 0 \\ 0 & 0 & 0 & 0 & 0 & 1/l_c^2 & 0 \\ 0 & 0 & 0 & 0 & 0 & 0 & 1/l_c^2 \end{bmatrix}. \tag{8}$$

The constitution of P ensures that in absence of couple-stresses ($m_{13} = m_{23} = 0$), $\sigma_{12} = \sigma_{21}$, the classical Von-Mises plasticity model is retrieved. At the same time this reveals one of the limitations of the Cosserat continuum. The regularising effect vanishes when no couple stresses are present. For an associated flow rule the plastic strain rate tensor is obtained from

$$\dot{\varepsilon}^{pl} = \dot{\lambda} \frac{\partial \Phi^{pl}}{\partial \boldsymbol{\sigma}}, \tag{9}$$

as in a standard continuum, with $\dot{\lambda}$ the rate of plastic multiplier. If we define the time derivative of the hardening/softening parameter κ as

$$\dot{\kappa} = ((2/3)(\dot{\varepsilon}^{pl})^T \boldsymbol{P} \dot{\varepsilon}^{pl})^{1/2}, \tag{10}$$

we obtain:

$$\dot{\kappa} = \dot{\lambda}. \tag{11}$$

which is also obtained for a classical continuum.

3
Strain softening visco-plasticity

As a second regularisation technique we shall employ a visco-plastic continuum model for which we shall briefly recall the basic equations (Simo et al. 1988; Loret and Prevost 1990; Sluys 1992). In this study we shall utilise the Duvaut–Lions (Duvaut and Lions 1922) model of visco-plasticity, according to which the rate dependent response of the continuum is defined by:

$$\dot{\varepsilon}^{vp} = \frac{H(\Phi^{pl})}{\eta} [D^{el}]^{-1} (\boldsymbol{\sigma} - \boldsymbol{\sigma}_n) \tag{12}$$

and

$$\dot{\kappa}^{vp} = -\frac{H(\Phi^{pl})}{\eta} (\kappa - \kappa_n) \tag{13}$$

where $\dot{\varepsilon}^{vp}$ is the visco-plastic strain rate, $\dot{\kappa}^{vp}$ the visco-plastic hardening/softening parameter, η the relaxation time and H is a step function ($H(\Phi^{pl}) = 1$ if $\Phi^{pl} > 0$ else $H(\Phi^{pl}) = 0$). $\boldsymbol{\sigma}_n$ is the projection of the trial stress vector on the yield surface in rate independent plasticity. In Eq. (13) κ_n is the rate independent hardening/softening parameter of which the rate is again defined by Eq. (10), but now with

$$P = \begin{bmatrix} 2/3 & -1/3 & -1/3 & 0 \\ -1/3 & 2/3 & -1/3 & 0 \\ -1/3 & -1/3 & 2/3 & 0 \\ 0 & 0 & 0 & 2 \end{bmatrix}. \tag{14}$$

Using additive strain decomposition and denoting $\dot{\varepsilon}^{el}$ as the elastic strain rate, the total strain rate in time step i can be expressed as:

$$\dot{\boldsymbol{\varepsilon}}_{(i)} = \dot{\boldsymbol{\varepsilon}}^{el}_{(i)} + \dot{\boldsymbol{\varepsilon}}^{vp}_{(i)}. \tag{15}$$

As a consequence we may write for the stress rate $\dot{\sigma}_{(i)}$

$$\dot{\sigma}_{(i)} = D(\dot{\varepsilon}_{(i)} - \dot{\varepsilon}^{vp}_{(i)}) \tag{16}$$

with the matrix D defining the elastic stress strain behaviour. If we integrate Eq. (16) over the time we obtain for the incremental stress tensor

$$\Delta\sigma_{(i)} = D(\Delta\varepsilon_{(i)} - \Delta\varepsilon^{vp}_{(i)}) \tag{17}$$

with the incremental visco-plastic strain tensor determined as:

$$\Delta\varepsilon^{vp}_{(i)} = \Delta t((1-\Theta)\dot{\varepsilon}^{vp}_{(i)} + \Theta\dot{\varepsilon}^{vp}_{(i+1)}) \tag{18}$$

where Θ is an integration constant; $0 \leqq \Theta \leqq 1$. Δt is the time interval for step $i(\Delta t = t_{(i+1)} - t_{(i)})$. The unknown visco-plastic strain rate at $\dot{\varepsilon}^{vp}_{(i+1)}$ can be approximated by a Taylor's series expansion, truncated after the linear terms:

$$\dot{\varepsilon}^{vp}_{(i+1)} = \dot{\varepsilon}^{vp}_{(i)} + \frac{\partial\dot{\varepsilon}^{vp}_{(i)}}{\partial\sigma}\Delta\sigma_{(i)} + \frac{\partial\dot{\varepsilon}^{vp}_{(i)}}{\partial\sigma_n}\Delta\sigma_{n,(i)}. \tag{19}$$

With the definition of the visco-plastic strain rate as in Eq. (12) this expression can be elaborated as follows:

$$\dot{\varepsilon}^{vp}_{(i+1)} = \dot{\varepsilon}^{vp}_{(i)} + \frac{1}{\eta}[D^{el}]^{-1}(\Delta\sigma_{(i)} - \Delta\sigma_{n,(i)}). \tag{20}$$

If we introduce this result in Eq. (18) the visco-plastic strain increment becomes

$$\Delta\varepsilon^{vp}_{(i)} = \left(\dot{\varepsilon}^{vp}_{(i)} + \frac{\Theta}{\eta}[D^{el}]^{-1}(\Delta\sigma_{(i)} - \Delta\sigma_{n,(i)})\right)\Delta t \tag{21}$$

which after substituting in Eq. (17) yields the final stress increment $\Delta\sigma_{(i)}$:

$$\Delta\sigma_{(i)} = D^{vp}_{(i)}\Delta\varepsilon_{(i)} - \Delta q^{vp}_{(i)} \tag{22}$$

where

$$D^{vp}_{(i)} = \frac{\eta}{\eta + \Theta\Delta t}D^{el} \tag{23}$$

and

$$\Delta q^{vp}_{(i)} = \frac{\eta}{\eta + \Theta\Delta t}\left(D^{el}\dot{\varepsilon}^{vp}_{(i)}\Delta t - \frac{\Theta\Delta t}{\eta}\Delta\sigma_{n,(i)}\right). \tag{24}$$

The vector $\Delta q^{vp}_{(i)}$ is an incremental "pseudo load" vector which has to be added to the right hand side of the equilibrium equations. The value of κ at $t = t_{(i+1)}$ is determined using the closed form solution of Simo (Simo et al. 1988) and is given by

$$\kappa_{(i+1)} = \kappa_{(i)}e^{-(\Delta t/\eta)} + (1 - e^{-(\Delta t/\eta)})\kappa_n. \tag{25}$$

4
Numerical modelling of the fibre-matrix interface

In this section a formulation of interface elements is presented and an orthotropic softening plasticity model is described which defines the relation between strength and stiffness degradation and crack opening in the interface elements (Schellekens 1992).

4.1
Interface element formulation

We consider a *nno*-noded line interface element as presented in Fig. 2. In a 2D configuration each node has two translational degrees-of-freedom, a_n and a_t, normal and tangential to the interface side respectively. In the case that the interface elements are used together with Cosserat continuum elements an additional rotational degree of freedom has to be added to each element node. This leads to an element nodal displacement vector a

$$a = (a_n^1, a_n^2, \ldots, a_n^{nno}, a_t^1, a_t^2, \ldots, a_t^{nno}, \omega_3^1, \omega_3^2, \ldots, \omega_3^{nno})^T, \tag{26}$$

where n denotes the direction normal to the interface surface and t denotes the direction tangential to the interface surface as can be seen in Fig. 2. The continuous displacement field is denoted as

$$u = (u_n^u, u_n^l, u_t^u, u_t^l)^T \tag{27}$$

where the superscripts u and l indicate the upper and lower side or plane of the interface respectively. With aid of the interpolation polynomials $n = (N_1, N_2, \ldots, N_{nno/2})^T$ the relation between the continuous displacement field and the nodal displacement vector is derived as

$$u = Ha \tag{28}$$

in which H contains the interpolation polynomials according to

$$H = \begin{bmatrix} n & 0 & 0 & 0 & ln & 0 \\ 0 & n & 0 & 0 & 0 & ln \\ 0 & 0 & n & 0 & 0 & 0 \\ 0 & 0 & 0 & n & 0 & 0 \end{bmatrix}. \tag{29}$$

The scalar l is the length of the element. To relate the continuous displacement field to the relative displacements an operator matrix L is introduced

$$L = \begin{bmatrix} -1 & +1 & 0 & 0 \\ 0 & 0 & -1 & +1 \end{bmatrix}. \tag{30}$$

When the relative displacement vector v is defined as $v = (v_n, v_t)^T$ we obtain

$$v = Lu. \tag{31}$$

The relation between nodal displacements and relative displacements for interface elements is now derived from Eqs. (28) and (31) as

$$v = LHa \rightarrow v = Ba \tag{32}$$

where the relative displacement-nodal displacement matrix B reads

$$B = \begin{bmatrix} -n & n & 0 & 0 & -ln & ln \\ 0 & 0 & -n & n & 0 & 0 \end{bmatrix}. \tag{33}$$

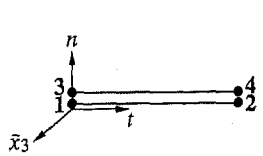

linear line interface

a

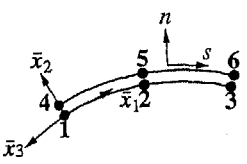

quadratic line interface

b

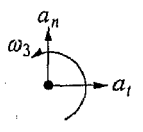

nodal degrees of freedom

c

Fig. 2. Line interface elements

If we consider an element in which the local coordinate systems in the integration points coincide with the global coordinate system, no transformations are necessary. For an arbitrary oriented interface element the matrix B has to be transformed to the local tangential coordinate system of the integration point or node-set. If the matrix R contains the local coordinate axes in the integration point, the transformation of the matrix B_g from the global coordinate system to the local axes (B_l) in the integration point is given by $B_l = B_g R^T$.

When the matrix D_I is used to denote the relation that describes the elastic constitutive behaviour of the interface element

$$D_I = \begin{bmatrix} d_n & 0 \\ 0 & d_t \end{bmatrix} \tag{34}$$

the traction-relative displacement relation becomes

$$t = D_I v \tag{35}$$

in which $t = (t_n, t_t)^T$ represents the traction vector.

In interface elements tractions and relative displacements are evaluated between the upper and the lower interface sides or planes. The components of the traction and relative displacement vector are determined by the orientations of the element sides, and are thus fixed. The virtual work equation for an interface element can be written as

$$\delta W = \int_S \delta v_{(j)}^T t_{(j)} \, dS \tag{36}$$

with S the surface of the interface element. In a nonlinear analysis the traction vector at the end of an iteration j can be expressed as

$$t_{(j)} = t_{(j-1)} + D_I^t \, dv_{(j)} \tag{37}$$

where $dv_{(j)}$ denotes the iterative change in the relative displacement vector, and D_I^t is now a properly linearised tangent operator. It can be demonstrated that variation of the relative displacement vector results in $\delta v_{(j)} = \delta(dv_{(j)})$. Introducing Eq. (37) in the virtual work expression and invoking (32) yields

$$\delta(da_{(j)})^T \int_S B^T D_I^t B \, dS \, da_{(j)} = -\delta(da_{(j)})^T \int_S B^T t_{(j-1)} \, dS. \tag{38}$$

The element stiffness matrix K and the internal force vector $f_{(j-1)}$ are now defined as

$$K = \int_S B^T D_I^t B \, dS \quad \text{and} \quad f_{(j-1)} = -\int_S B^T t_{(j-1)} \, dS. \tag{39}$$

For numerically integrated interface elements the integrals in Eq. (39) are replaced by an integration over the iso-parametric coordinates ξ and η. For the element stiffness matrix this gives

$$K = b \int_{\xi=-1}^{\xi=+1} B^T D_I^t B \left(\left(\frac{\partial x_1}{\partial \xi} \right)^2 + \left(\frac{\partial x_2}{\partial \xi} \right)^2 \right)^{1/2} d\xi. \tag{40}$$

where b is the width of the interface.

4.2
A constitutive model for interface debonding

For the modelling of mode-I interface fracture the discrete crack model described in Rots (1988) is sufficient. However, when the fracture in the interface is not purely of a mode-I type, and energy is also released in mode-II and mode-III, this discrete crack model is no longer applicable (Schellekens 1992). To describe mixed-mode failure a constitutive model is required in which both components of the traction vector t are involved. An orthotropic hardening/softening plasticity model now is proposed for the modelling of mixed-mode fracture in composities. The yield condition for interface plasticity is given by

$$\Phi^{pl}(t, \kappa) = C_{nn} t_n^2 + C_{tt} t_t^2 + C_n t_n - \bar{t}^2(\kappa) = 0 \tag{41}$$

with C_{ii} and C_{ij} a set of material constants, $\bar{t}$ a normalised yield traction and κ the hardening/softening parameter. t_n and t_t are the components of the traction vector. If $\bar{t}_n^c$ and $\bar{t}_n^t$ denote the compressive and tensile yield tractions in the direction normal to the interface side and if $\bar{t}_t$ is the shear yield traction we obtain:

$$C_{nn}=\frac{\bar{t}^2}{\bar{t}_n^t\bar{t}_n^c}\quad C_{tt}=\frac{\bar{t}^2}{\bar{t}_n^2}\quad C_n=\frac{\bar{t}^2}{\bar{t}_n^t}-\frac{\bar{t}^2}{\bar{t}_n^c}. \tag{42}$$

Recasting Eq. (41) in matrix-vector notation yields

$$\Phi^{pl}(t,\kappa)=\frac{1}{2}t^TPt+t^TP-\bar{t}^2(\kappa)=0 \tag{43}$$

in which $t^T=(t_n,t_t)$, $P=\mathrm{diag}(2C_{nn},2C_{tt})$ and $p^T=(C_n,0)$.

As soon as this condition is satisfied, the total relative displacement rate $\dot{v}$ is decomposed into an "elastic" part, $\dot{v}^{el}$, and a "plastic" part, $\dot{v}^{pl}$, as follows:

$$\dot{v}=\dot{v}^{el}+\dot{v}^{pl}. \tag{44}$$

The elastic relative displacement rate is related to the traction rate by

$$\dot{t}=\mathrm{D}_I\dot{v}^{el}, \tag{45}$$

and the assumption of an associated flow rule yields for the plastic relative displacement rate:

$$\dot{v}^{pl}=\dot{\lambda}\frac{\partial\Phi^{pl}}{\partial t}. \tag{46}$$

For the present orthotropic yield criterion (43) this gives:

$$\dot{v}^{pl}=\dot{\lambda}(Pt+p). \tag{47}$$

Furthermore, the scalar κ in the case of a work hardening/softening hypothesis reads

$$\kappa=\int\dot{\kappa}\,dt\quad\text{with}\quad\dot{\kappa}=t^T\dot{v}^{pl}. \tag{48}$$

4.2.1
Integration of the elasto-plastic relations

For finite increments of loading, Eqs. (44) to (48) can be recast as:

$$\Delta v_{(j)}=\Delta v_{(j)}^{el}+\Delta v_{(j)}^{pl} \tag{49}$$

$$\Delta v_{(j)}^{el}=D_I^{-1}\Delta t_{(j)} \tag{50}$$

$$\Delta v_{(j)}^{pl}=\Delta\lambda_{(j)}(Pt_{(j)}+p) \tag{51}$$

$$\Delta\kappa_{(j)}=t_{(j)}^T\Delta v_{(j)}^{pl}. \tag{52}$$

A combination of these relations yields

$$D_I^{-1}\Delta t_{(j)}-\Delta v_{(j)}+\Delta\lambda_{(j)}(Pt_{(j)}+p)=0 \tag{53}$$

and finally

$$t_{(j)}=(D_I^{-1}+\Delta\lambda_{(j)}P)^{-1}(v_{(i)}^{el}+\Delta v_{(j)}-\Delta\lambda_{(j)}p). \tag{54}$$

Substitution of this expression for $t_{(j)}$ in the yield condition (43) results in a nonlinear equation in $\Delta\lambda_{(j)}$: $\Phi^{pl}(\Delta\lambda_{(j)})=0$, which can be solved by a local Newton–Raphson procedure:

$$\Delta\lambda_{(j)}^{k+1} = \Delta\lambda_{(j)}^{k} - \left.\frac{\Phi^{pl}}{\dfrac{\partial \Phi^{pl}(\Delta\lambda)}{\partial \Delta\lambda}}\right|_{\Delta\lambda_{(j)}^{k}} \tag{55}$$

in which k is the local iteration number. The derivative of $\Phi^{pl}(\Delta\lambda_{(j)})$ with respect to $\Delta\lambda_{(j)}$ in Eq. (55) reads

$$\frac{\partial \Phi^{pl}(\Delta\lambda_{(j)})}{\partial \Delta\lambda_{(j)}} = \left(\frac{\partial \Phi^{pl}}{\partial t_{(j)}}\right)^{T} \frac{\partial t_{(j)}}{\partial \Delta\lambda_{(j)}} + \frac{\partial \Phi^{pl}}{\partial \kappa}\frac{\partial \kappa}{\partial \Delta\lambda_{(j)}} \tag{56}$$

and can be elaborated to give:

$$\frac{\partial \Phi^{pl}(\Delta\lambda_{(j)})}{\partial \Delta\lambda_{(j)}} = -(\boldsymbol{P}\boldsymbol{t}_{(j)} + \boldsymbol{p})^{T}(\boldsymbol{D}_{I}^{-1} + \Delta\lambda_{(j)}\boldsymbol{P})^{-1}((\boldsymbol{D}_{I}^{-1} + \Delta\lambda_{(j)}\boldsymbol{P})^{-1}\boldsymbol{P}$$

$$\cdot(\boldsymbol{v}_{(i)}^{el} + \Delta\boldsymbol{v}_{(j)} - \Delta\lambda_{(j)}\boldsymbol{p}) + \boldsymbol{p}) - h, \tag{57}$$

where

$$h = -\left.\frac{\partial \Phi^{pl}}{\partial \kappa}\boldsymbol{t}^{T}\frac{\partial \Phi^{pl}}{\partial \boldsymbol{t}}\right|_{t_{(j)}}, \tag{58}$$

is the hardening/softening modulus. The hardening/softening parameter κ is then updated according to

$$\Delta\kappa_{(j)} = \Delta\lambda_{(j)}\boldsymbol{t}_{(j)}^{T}(\boldsymbol{P}\boldsymbol{t}_{(j)} + \boldsymbol{p}). \tag{59}$$

4.2.2
The consistent tangent operator for orthotropic plasticity

The derivation of the consistent tangent stiffness relation for orthotropic hardening/softening plasticity in interface elements is outlined below. Due to the hardening or softening type of response additional terms occur in the nonlinear equations which eventually results in a non-symmetric tangent stiffness relation.

The total relative displacement vector at the end of iteration j is given by

$$\boldsymbol{v}_{(j)} = \boldsymbol{v}_{(i)} + \Delta\boldsymbol{v}_{(j)}^{el} + \Delta\boldsymbol{v}_{(j)}^{pl} \tag{60}$$

where $\boldsymbol{v}_{(i)}$ is the relative displacement vector at the beginning of the time step. With the relations for the incremental elastic and plastic relative displacements

$$\Delta\boldsymbol{v}_{(j)}^{el} = \boldsymbol{D}_{I}^{-1}(\boldsymbol{t}_{(j)} - \boldsymbol{t}_{(i)}) \quad \text{and} \quad \Delta\boldsymbol{v}_{(j)}^{pl} = \Delta\lambda_{(j)}\frac{\partial \Phi^{pl}}{\partial \boldsymbol{t}_{(j)}} \tag{61, 62}$$

the traction-relative displacement relation can be written as

$$\boldsymbol{v}_{(j)} = \boldsymbol{v}_{(i)} + \boldsymbol{D}^{-1}(\boldsymbol{t}_{(j)} - \boldsymbol{t}_{(i)}) + \Delta\lambda_{(j)}\frac{\partial \Phi^{pl}}{\partial \boldsymbol{t}_{(j)}}. \tag{63}$$

The time derivative of Eq. (63) reads

$$\dot{\boldsymbol{v}}_{(j)} = \boldsymbol{D}_{I}^{-1}\dot{\boldsymbol{t}}_{(j)} + \Delta\lambda_{(j)}\frac{\partial^{2} \Phi^{pl}}{\partial \boldsymbol{t}_{(j)}^{2}}\dot{\boldsymbol{t}}_{(j)} + \dot{\lambda}\frac{\partial \Phi^{pl}}{\partial \boldsymbol{t}_{(j)}}. \tag{64}$$

Introducing the relation for the plastic relative displacement rate in the consistency condition

$$\dot{\Phi}^{pl} = \left(\frac{\partial \Phi^{pl}}{\partial \boldsymbol{t}}\right)^{T}\dot{\boldsymbol{t}} + \frac{\partial \Phi^{pl}}{\partial \kappa}\dot{\kappa} = 0 \tag{65}$$

leads to

$$\dot{\Phi}^{pl} = \left(\frac{\partial \Phi^{pl}}{\partial t_{(j)}}\right)^T \dot{t}_{(j)} + \Delta\lambda_{(j)} \frac{\partial \Phi^{pl}}{\partial \kappa}\left(\frac{\partial \kappa}{\partial v^{pl}_{(j)}}\right)^T \frac{\partial^2 \Phi^{pl}}{\partial t^2_{(j)}} \dot{t}_{(j)} + \dot{\lambda}_{(j)} \frac{\partial \Phi^{pl}}{\partial \kappa}\left(\frac{\partial \kappa}{\partial v^{pl}_{(j)}}\right)^T \frac{\partial \Phi^{pl}}{\partial t_{(j)}} = 0. \tag{66}$$

From this relation the time derivative of the plastic multiplier $\dot{\lambda}$ can be solved to be

$$\dot{\lambda}_{(j)} = \frac{1}{h}\left(\left(\frac{\partial \Phi^{pl}}{\partial t_{(j)}}\right)^T + \Delta\lambda_{(j)} \frac{\partial \Phi^{pl}}{\partial \kappa}\left(\frac{\partial \kappa}{\partial v^{pl}_{(j)}}\right)^T \frac{\partial^2 \Phi^{pl}}{\partial t^2_{(j)}}\right) \dot{t}_{(j)} \tag{67}$$

in which h is given by Eq. (58). Substituting the above expression for $\dot{\lambda}$ in Eq. (66) subsequently yields for the relative displacement rate $\dot{v}_{(j)}$

$$\dot{v}_{(j)} = \left[D_I^{-1} + \Delta\lambda_{(j)} \frac{\partial^2 \Phi^{pl}}{\partial t^2_{(j)}} + \frac{1}{h} \frac{\partial \Phi^{pl}}{\partial t_{(j)}}\left(\frac{\partial \Phi^{pl}}{\partial t_{(j)}}\right)^T + \frac{\Delta\lambda_{(j)}}{h} \frac{\partial \Phi^{pl}}{\partial \kappa}\left(\frac{\partial \Phi^{pl}}{\partial t_{(j)}}\right)\left(\frac{\partial \kappa}{\partial v^{pl}_{(j)}}\right)^T \frac{\partial^2 \Phi^{pl}}{\partial t^2_{(j)}} \right] \dot{t}_{(j)}. \tag{68}$$

At this point a matrix H is introduced

$$H = D_I^{-1} + \Delta\lambda_{(j)} \frac{\partial^2 \Phi^{pl}}{\partial t^2_{(j)}} + \frac{\Delta\lambda_{(j)}}{h} \frac{\partial \Phi^{pl}}{\partial \kappa}\underline{\left(\frac{\partial \Phi^{pl}}{\partial t_{(j)}}\right)\left(\frac{\partial \kappa}{\partial v^{pl}_{(j)}}\right)^T} \frac{\partial^2 \Phi^{pl}}{\partial t^2_{(j)}}. \tag{69}$$

The underlined part in Eq. (69) introduces the non-symmetry in the matrix H, which renders the tangential stiffness matrix to be non-symmetric (see Eq. (71)). With Eq. (69), Eq. (68) can conveniently be rewritten as

$$\dot{v}_{(j)} = \left[H + \frac{1}{h} \frac{\partial \Phi^{pl}}{\partial t_{(j)}}\left(\frac{\partial \Phi^{pl}}{\partial t_{(j)}}\right)^T \right] \dot{t}_{(j)}. \tag{70}$$

Use of the Sherman–Morrison–Woodbury formula then yields the consistent tangent stiffness relation

$$\dot{t}_{(j)} = \left[H^{-1} - \frac{H^{-1}\left(\frac{\partial \Phi^{pl}}{\partial t_{(j)}}\right)\left(\frac{\partial \Phi^{pl}}{\partial t_{(j)}}\right)^T H^{-1}}{h + \left(\frac{\partial \Phi^{pl}}{\partial t_{(j)}}\right)^T H^{-1}\left(\frac{\partial \Phi^{pl}}{\partial t_{(j)}}\right)} \right] \dot{v}_{(j)}. \tag{71}$$

4.3
Assumptions for the debonding model

Due to the fact that we intend to model both plasticity and craking in the interface we can no longer regard the inelastic deformations (v^{pl}) as being purely plastic. Therefore, we define the inelastic relative displacements as crack relative displacements (v^{cr}) except for the mode-I inelastic relative

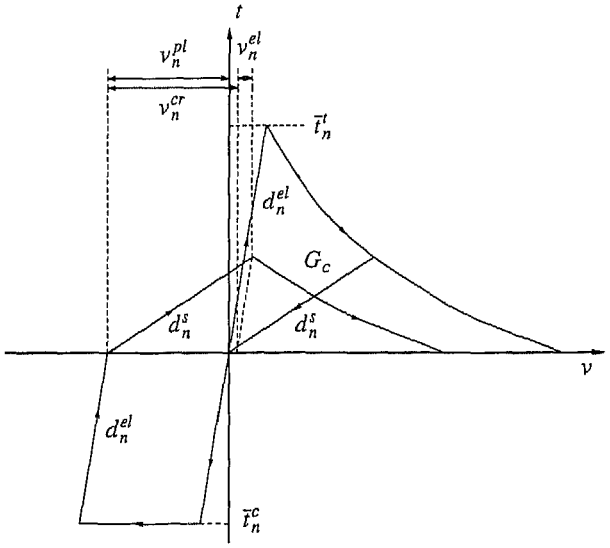

Fig. 3. Traction relative displacement diagram for the mode-I component (d_n^{el} and d_n^s denote the elastic and secant stiffness respectively)

displacements that are induced by a compressive loading. These are considered as plastic (see Fig. 3). The degradation of the elastic properties of the interface is coupled with the inelastic relative displacement due to cracking ($\mathbf{v}^{cr}$). In this case the stiffness that determines the tractions in unloading or reloading is the so-called secant stiffness matrix denoted by D_I^s. From the moment of crack-closure (defined by $v_n \leqq v_n^{pl}$), that is in the compressive loading regime, the initial elastic stiffness governs the interface behaviour. For the calculations shown in this contribution, it is assumed that due to the irreversible plastic relative displacements that may occur, the traction relative displacement diagram shifts horizontally over a distance v_n^{pl} (see Fig. 3). Furthermore the assumption is made that degradation of the equivalent yield traction $\bar{t}$ is not influenced by yielding in compression. Thus the amount of inelastic work that is used to determine the values of $\bar{t}$ and C_n is defined as $\kappa = \int \mathbf{t}^T \dot{\mathbf{v}}^{cr}\, dt$. In the analyses that are presented in the next section a linear relation between κ and $\bar{t}$ has been assumed:
78 $\bar{t} = \bar{t}_0(1 - \kappa/G_c)$, where $\bar{t}_0$ denotes the initial transverse tensile strength of the interface and G_c denotes the fracture toughness of the interface. A physical interpretation of the work-softening model is that once the fracture toughness of the interface has been released as free-surface energy, the strength and stiffness of the interface will have completely reduced to zero.

5
Analyses of matrix fracture and debonding

Since a poor bonding between fibres and matrix limits the possibilities of composites that contain high performance fibres, at present much effort is put in understanding the interaction between fibres and matrix and improving the interface bonding. In this section we shall present the results of micro-mechanical analyses of matrix fracture and the interaction between matrix fracture and fibre-matrix debonding. In the analyses the fibres and the matrix are modelled as a visco-plastic continuum and as a micro-polar Cosserat continuum. Special interface elements are used to provide the bond between the fibres and the matrix. For the matrix a linear relation between the equivalent

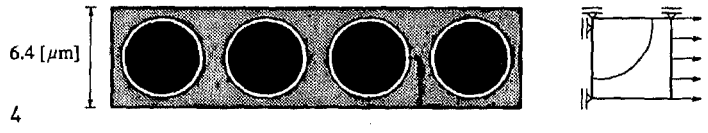

4

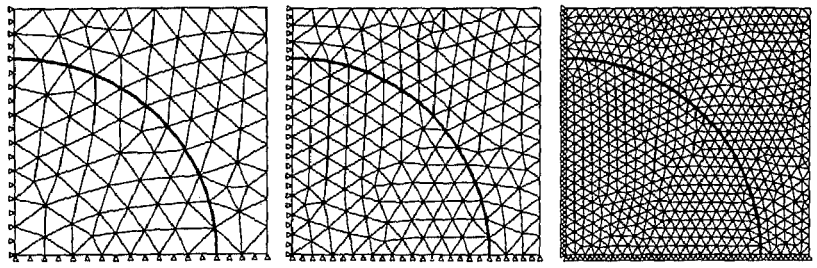

5

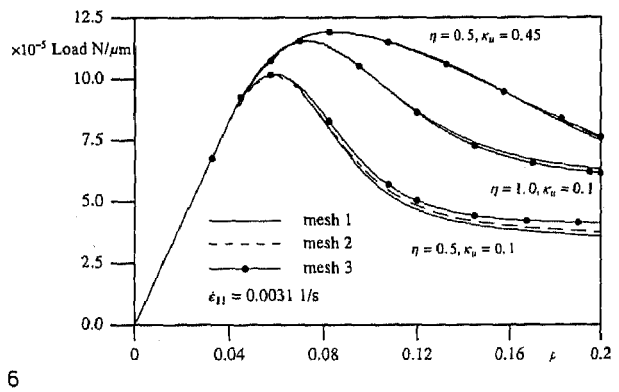

6

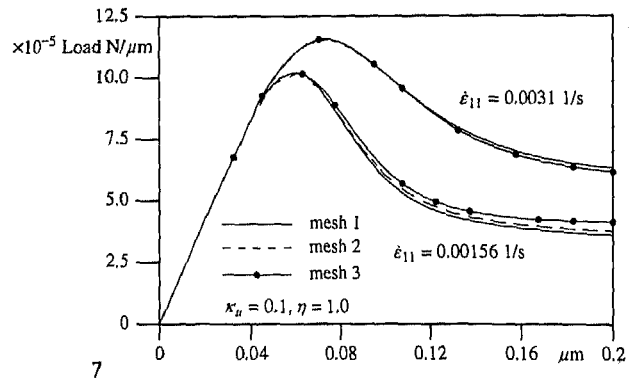

7

Figs. 4–7. 4 Geometry of the reference volume element. 5 Finite element discretisation of RVE. 6 Load displacement curves for the right boundary. Effects of variation of η and κ_u. 7 Load displacement curves for the right boundary. Influence of the strain rate on the RVE response

yield stress ($\bar{\sigma}$) and the softening parameter is assumed ($\bar{\sigma} = \bar{\sigma}_0(1 - \kappa/\kappa_u)$). First the results for the visco-plastic continuum modelling are discussed followed by the results from analyses in which the Cosserat continuum is applied.

5.1
Micro-mechanical analyses using visco-plasticity

We start with the investigation of matrix fracture in a carbon-epoxy composite. In the composite we assume a periodic arrangement of the fibres which results in a natural choice for the reference volume element (RVE). The uni-directional composite (50% fibre volume fraction) is loaded in transverse tension as shown in Fig. 4. The material properties for the Apollo IM 43-750 carbon fibres and the Ciba-Geigy Araldite Epoxy matrix are listed in Table 1. Also the material properties for the interface elements, which enter the model at a later stage, are included in Table 1.

Table 1. Properties for the matrix, fibres and the interface

	Fibres	Matrix	Interface elements	
E [N/mm²]	12000	3200	d_n, d_t [N/mm³]	100.0
ν	0.3	0.37	$\bar{t}_0 = \bar{t}_n^t$ [N/mm²]	85.0
$\bar{\sigma}_0$ [N/mm²]	—	85.0	$\bar{t}_n^c = \bar{t}_n$ [N/mm²]	85.0
κ_u [mm/mm]	—	0.1	G_c [J/m²]	100.0

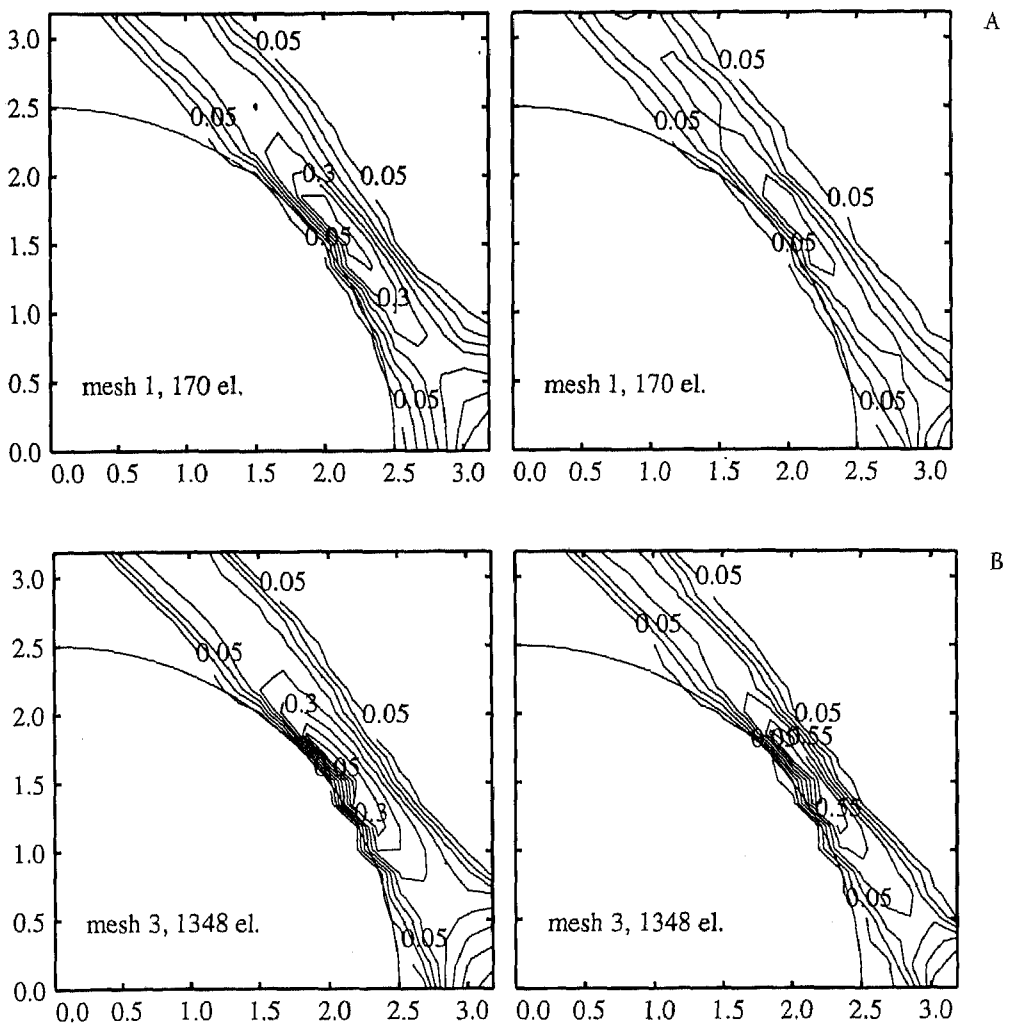

Fig. 8. A Contour plots of equivalent plastic strains for mesh 1 at a displacement of 0.2 μm. Left diagram: $\dot{\varepsilon}_{11} = 0.0031$ 1/s. Right diagram: $\dot{\varepsilon}_{11} = 0.00156$ 1/s. B Contour plots of equivalent plastic strains for mesh 3 at a displacement of 0.2 μm. Left diagram: $\dot{\varepsilon}_{11} = 0.0031$ 1/s. Right diagram: $\dot{\varepsilon}_{11} = 0.00156$ 1/s

Due to symmetry only a quarter of the RVE was discretised using 170 (mesh 1), 336 (mesh 2) and 1348 (mesh 3) quadratic plane-strain triangles respectively, as is shown in Fig. 5. In the vertical direction free contraction of the RVE is allowed whereas an equal displacement constraint was imposed on the nodes of the right boundary. The response of the three meshes was calculated taking different values for the relaxation time η, the ultimate value for the softening parameter κ_u and for the loading rate $\dot{\varepsilon}_{11}$.

The results of the mesh-refinement study are presented in Figs. 6 and 7 in terms of load-displacement curves for the right boundary of the RVE. We observe that the response of the RVE converges to a unique solution upon mesh refinement. This is the result of the regularising effect of the visco-plastic continuum model. Furthermore Figs. 6 and 7 show that for decreasing loading rates and for the lower value of the relaxation time the difference in response of the three discretisation slightly increases. This is explainable since for the limit cases of $\dot{\varepsilon}_{11} \to 0$ and $\eta \to 0$ respectively, the standard (mesh-sensitive) continuum solution is obtained. Figures 8A and 8B present the contour plots the equivalent plastic strains in meshes 1 and 3 corresponding to the curves of Fig. 7. It is shown that the width of the localisation band remains finite and approximately constant upon mesh-refinement, although a slight decrease in width is observed for the right diagrams which correspond to the lower loading rate.

In the next series of analyses the attention is focused on the interaction between fibre-matrix debonding and matrix fracture. At this point the interface elements are introduced in the finite element

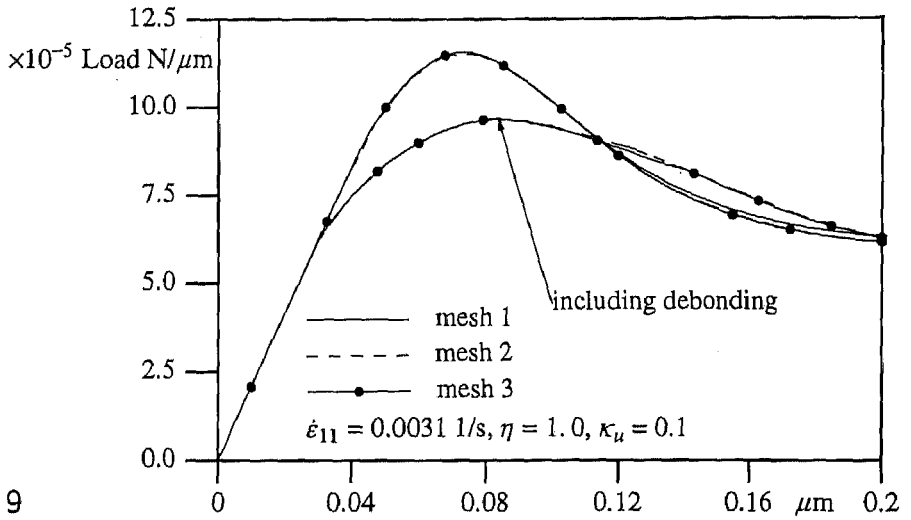

9

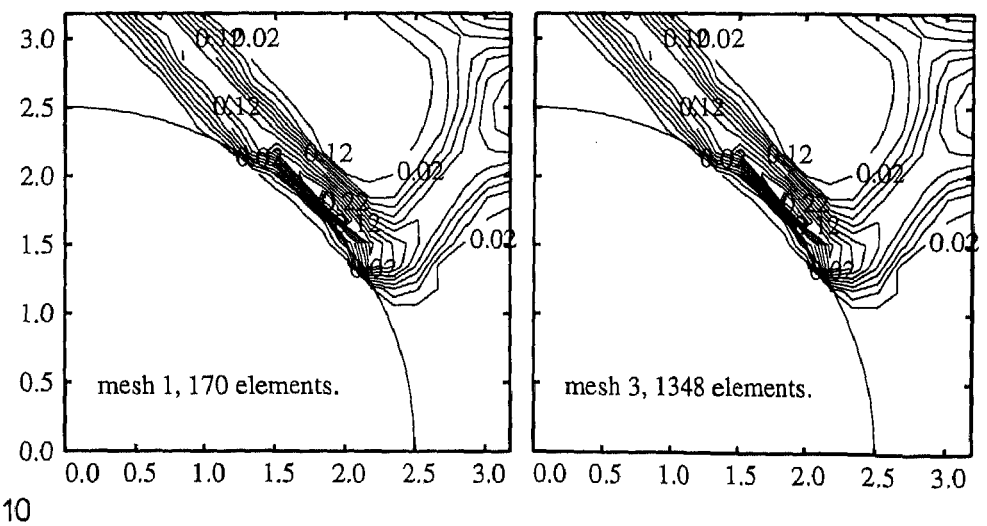

10

Figs. 9–10. 9 Load displacement curves for the right boundary. Influence of fibre matrix debonding on the RVE-response. 10 Contour plots of equivalent plastic strains at a displacement of 0.2 μm. Strain rate 0.0031 1/s. $\eta = 1.0$, $\kappa_u = 0.1$

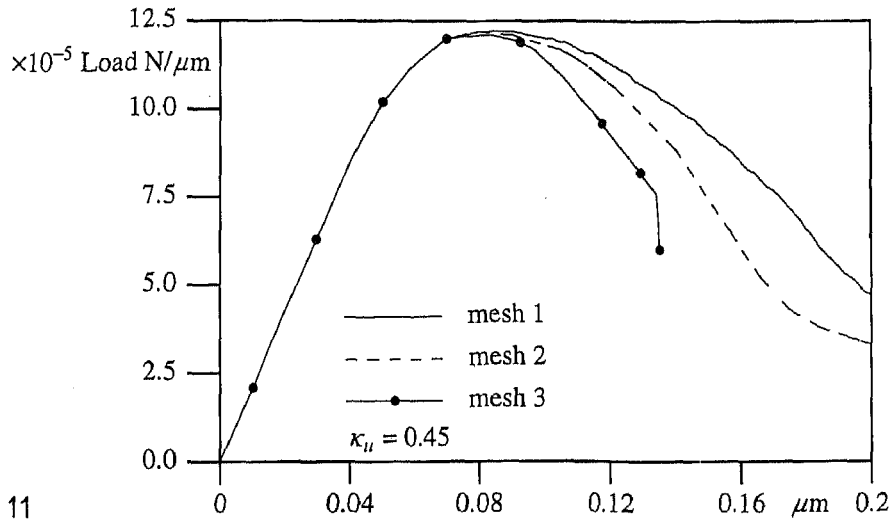

11

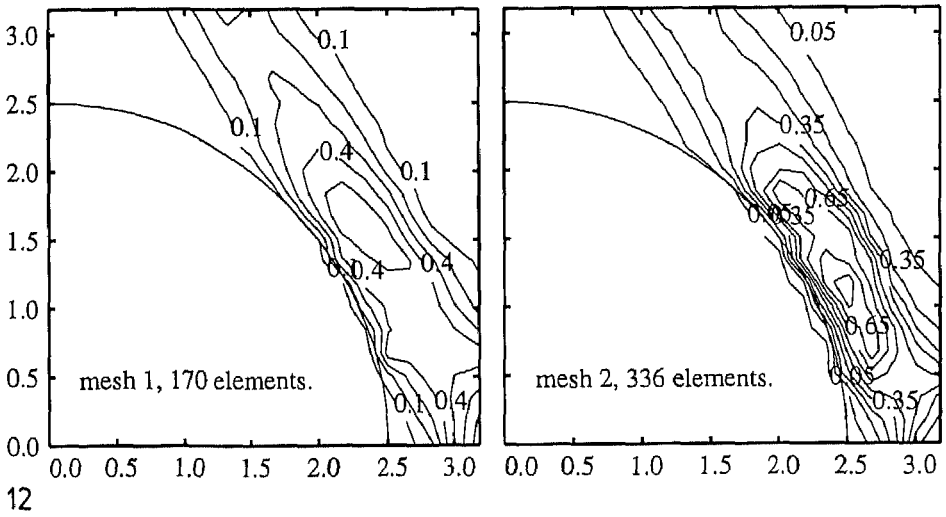

12

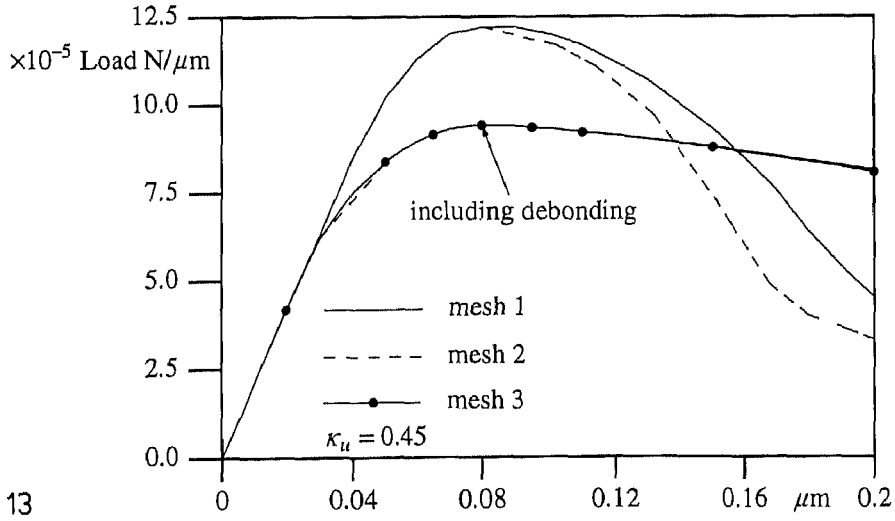

13

Figs. 11–13. 11 Load displacement curves for the right boundary using a Cosserat continuum. 12 Contour plots of equivalent plastic strains for a Cosserat continuum. Displacement: 0.2 μm. 13 Load displacement curves for the right boundary using a Cosserat continuum

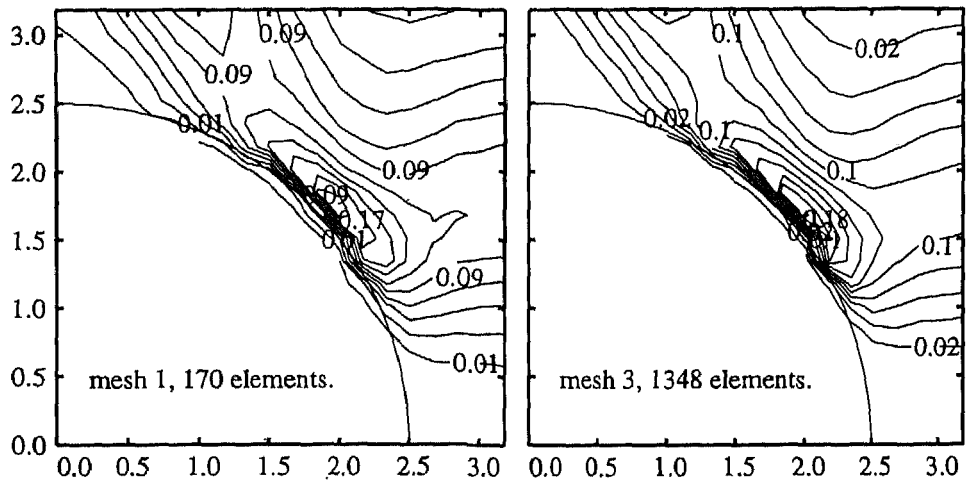

Fig. 14. Contour plots of equivalent plastic strains for a Cosserat continuum including interface elements. Displacement: 0.2 μm

model. The three meshes of Fig. 5 have been analysed again with the material data set specified in Table 1. Figure 9 shows the load displacement curves for the three discretisations. It is observed that when fibre-matrix debonding is taken into account the results also converge to the same solution. As a reference the results for perfect bonding have been included in Fig. 9 and it can be seen that the influence of the fibre-matrix bond strength on the response of the RVE is significant. Finally, the contour plots of the equivalent plastic strains (Fig. 10, meshes 1 and 3) demonstrate that size of the localisation zone is not affected by the mesh refinement. Hence mesh-insensitive results have been obtained for the analysis of the interaction between matrix fracture and debonding.

5.2
Micromechanical analyses using a Cosserat continuum model

In this section the results for the Cosserat continuum are discussed. For the length scale parameter of the Cosserat continuum model a value equal to $l_c = 0.25$ μm was chosen arbitrarily, whereas the Cosserat shear modulus μ_c for both the fibres and the matrix was chosen equal to their conventional shear modulus. The hardening/softening parameter κ_u was taken equal to 0.45.

Figure 11 presents the load displacement curves of the right boundary of the RVE for the different discretisations. We now observe that there is a distinct different in response upon mesh refinement. This is mainly the result of the fact that the mode-I component of the stress and strain vectors disturbs the regularising effect of the Cosserat model. Also the contour plots in Fig. 12 show mesh-sensitivity of the results. However the width of the localisation band remains finite and does not reduce to zero upon mesh-refinement, as is the case for a classical continuum.

However, the results for the analyses in which fibre-matrix debonding has been taken into account show exactly the opposite as can be seen in from Figs. 13 and 14. Here we show the load displacement curves and the contour plots for the Cosserat continuum including interfaces. Similar to the results for visco-plasticity presented in Sect. 5.1, a mesh-insensitive response of the RVE has been obtained using the Cosserat continuum.

References

Beer, G. 1985: An isoparametric joint/interface element for finite element analysis. Int. J. Num. Meth. Engng. 21: 585–600
Borst, R. de 1991: Simulation of strain localisation: A reappraisal of the Cosserat continuum. Engng. Comput. 8: 317–332
Cosserat, E.; Cosserat, F. 1909: Théorie des Corps Deformables. Herman et Fils, Paris
Duvaut, G.; Lions, J. L. 1922: Les Inequations en Mechanique et en Physique. Dunod, Paris
Goodman, R. E.; Taylor, R. L.; Brekke, T. L. 1968: A model for the mechanics of jointed rock. ASCE J. Soil Mech. Found. Div. 94: 637–659
Günther, W. 1958: Zur Statik und Kinematik des Cosseratschen Kontinuums. Abh. Braunschweig. Wiss. Ges. 10: 195–213
Larsson, R. 1990: Numerical simulation of plastic localisation. Publication 90: 5, Department of Structural Mechanics, Chalmers University of Technology, Goteborg
Loret, B.; Prevost, J. H. 1990: Dynamic strain localization in elasto-(visco-)plastic solids, Part 1. General formulation and one dimensional examples. Comp. Meth. Appl. Mech. Engng. 83: 247–273
Mühlhaus, H.-B.; Vardoulakis, I. 1987: The thickness of shear bands in granular materials. Geotechnique 37: 271–283

Mühlhaus, H.-B. 1988: Lamination phenomena in prestressed rock. Preprints 2nd Int. Symp. on Rockbursts and Seismicity in Mines. *University of Minnesota, Minneapolis, pp. 117–128*
Mühlhaus, H.-B. 1989: Application of Cosserat theory in numerical solutions of limit load problems. Ing.-Arch. 59: 124–137
Mühlhaus, H.-B. 1990: Continuum models for layered and blocky rock. Comprehensive rock engineering, Vol. 2: analysis and design methods, Pergamon Press, Oxford
Ngo, D.; Scordelis, A. C. 1967: Finite element analysis of reinforced concrete beams. J. Amer. Concrete Institute. 64: 152–163
Rots, J. G. 1988: Computational modelling of concrete fracture. Dissertation, Delft University of Technology, Delft
Schaefer, H. 1962: Versuch einer Elastizitätstheorie des zweidimensionalen ebenen Cosserat-Kontinuums, Miszellaneen der Angewandten Mechanik. Akademie-Verlag. Berlin, pp. 277–292
Schaefer, H. 1975: A contribution to the solution of contact problems with the aid of bond elements. Comp. Meth. Appl. Mech. Engng. 6: 335–354
Schellekens, J. C. J. 1992: Computational strategies for composite structures. Dissertation, Delft University of Technology, Delft
Schellekens, J. C. J.; Borst, R. de 1993a: On the integration of interface elements. Int. J. Num. Meth. Engng. 36: 43–66
Schellekens, J. C. J.; Borst, R. de 1993b: A non-linear finite element approach for the analysis of mode-I free edge delamination in composites. Int. J. Solids Structures 30(9): 1239–1253
Simo, J. C.; Kennedy, J. G.; Govindjee, S. 1988: Non-smooth multisurface plasticity and visco-plasticity-Loading/unloading conditions and numerical algorithms. Int. J. Num. Meth. Engng. 26: 2161–2185
Sluys, L. J. 1992: Wave propagation, localisation and dispersion in strain softening solids. Dissertation, Delft University of Technology, Delft